# We are IntechOpen, the world's leading publisher of Open Access books Built by scientists, for scientists

**4,800**
Open access books available

**122,000**
International authors and editors

**135M**
Downloads

Our authors are among the

**154**
Countries delivered to

**TOP 1%**
most cited scientists

**12.2%**
Contributors from top 500 universities

CLARIVATE ANALYTICS BOOK CITATION INDEX INDEXED

WEB OF SCIENCE™

Selection of our books indexed in the Book Citation Index in Web of Science™ Core Collection (BKCI)

## Interested in publishing with us?
## Contact book.department@intechopen.com

Numbers displayed above are based on latest data collected.
For more information visit www.intechopen.com

# 13

# Structural Characteristic and Superconducting Performance of $MgB_2$ Fabricated by Mg Diffusion Process

Minoru Maeda[1], Jung Ho Kim[2] and Shi Xue Dou[2]
[1]*Department of Physics, College of Science and Technology, Nihon University*
[2]*Institute for Superconducting and Electronic Materials,*
*Australian Institute of Innovative Materials, University of Wollongong*
[1]*Japan*
[2]*Australia*

## 1. Introduction

The phenomenon of superconductivity, which arises from an unusual quantum mechanism below a superconducting critical transition temperature ($T_c$), shows unique physical properties, namely, exactly zero direct current (dc) electrical resistance, the Meissner effect associated with nearly perfect diamagnetism, and the Josephson effect in two weakly coupled superconductors which may have applicability in high-speed, high-sensitivity, low-voltage sensors and switches. Thanks to these valuable characteristics, today, superconducting materials are having a considerable influence on the development of the next generation of medical services, electrical power systems, transportation, communication technology, and integrated circuits. Thus, our energy-hungry world increasingly requires those technologies and superconductors are becoming indispensable materials.

Superconductivity was discovered by Heike Kamerlingh Onnes in 1911. It is one of the greatest discoveries in the history of science. After that, he tried to fabricate a superconducting magnet using lead (Pb), but it failed. From the failure of his experiment, he learned of the existence of the critical field of superconductors, which completely suppresses superconductivity. His dream was that a high magnetic field could be excited by magnets using superconductors, but it was left unfulfilled. In 1947, a compact helium liquefier was invented by Collins and cowokers, and it made possible some advance in theoretical and experimental studies related to superconducting magnets. From 1960 to 1990, niobium titanium (NbTi) and niobium tin ($Nb_3Sn$) superconductors were employed in many kinds of approaches towards technical development for real applications. These efforts formed the basis of technical application for magnets using metallic superconducting materials, and even now, many researchers are still making steady progress on it. As a result, superconducting materials have become widely applied in not only research magnets for laboratory use, but also various other instruments, which is more than what was expected. Specifically, magnetic resonance imaging (MRI)

equipment provides image contrast between different kinds of soft issues in the human body and it is essential to confirm the diagnosis of spinal disc herniation, anterior cruciate ligament injury, tumour, and stroke. Nuclear magnetic resonance (NMR) equipment is utilized on the cutting edge of genome-related research. In addition, superconducting magnetic energy storage (SMES), magnetic levitation systems for transportation, and large-scale magnets for confinement of plasma in fusion reactors are expected as the next generation of devices for energy production, its storage, and its distribution, even though they are still at the experimental stage of development. On the other hand, cooling technology, which is crucial for superconducting applications, has also maintained steady progress for the past 15 years. The most recent helium liquefier has smaller scale, longer operation life, and higher energy-saving compared with those a decade ago. Small, convenient cryocoolers without liquid helium have been put to practical use and developed into lower power consumption versions. A unique small pulse tube refrigerator without moving pistons in the low-temperature part of the device is also coming into actual utilization and can easily achieve a low temperature of 10 ~ 20 K. Thus, the development of cooling technology has given an impulse to superconducting applications.

Despite the recent progress of cooling technology, today, the majority of current practical superconducting devices are still made of NbTi and $Nb_3Sn$ superconductors, which have the low $T_c$ values below 20 K. MRI is one of the conventional superconducting devices and has been critical to our high-quality healthcare. However, only 10 % of human beings utilize the superconducting technology in the world. The most serious cause of disturbing its largely widespread use is to need liquid Helium for activating MRI magnets at 4.2 K. The cryogen is expensive and unmanageable, and its resource is exhaustible. In order to promote its widespread use and reduce operating cost, the next generation of superconducting technology must eliminate the use of liquid cryogen bath cooling and its real application has been strongly required. Currently, the most promising materials are thought to be bismuth strontium calcium copper oxide (BSCCO), yttrium barium cooper oxide (YBCO), and magnesium diboride ($MgB_2$). $MgB_2$, a metallic compound, shows $T_c$ of ~ 39 K, the highest value that has been reported for conventional metallic superconductors, and its superconductivity was discovered by Jun Akimitsu's group in 2001 (Nagamatsu et al., 2001). Owing to its large thermal margin than Nb based superconductors, $MgB_2$ superconducting materials have been judged potentially capable of meeting the needs of the next-generation superconducting applications operated at 15~30 K. $MgB_2$ materials also show superior characteristics for industrial applications including that (1) the manufacture method is much easier to that of NbTi wires, (2) the raw materials are much cheaper than that of YBCO thin films and BSCCO wires, and the manufacturing cost would potentially be lower than that of NbTi wires, (3) the density is one third of NbTi and it can yield triple length wire using the same mass of raw materials, (4) the charging rate of the magnet is faster than that of NbTi magnet, (5) the lower anisotropy and the lager coherence length do not make the weak link problem severe compared with YBCO thin films and BSCCO wires (Larbalestier et al., 2001). Although the $T_c$ values of YBCO and BSCCO show 93 K and 110 K, respectively, and those are much higher than that of $MgB_2$, the prices of those conductors seem not to be reduced in spite of enormous efforts for more than 20 years. In these regards, therefore, $MgB_2$ materials have been energetically studied for industrial applications in the world since the discovery of the superconductivity.

## 2. $MgB_2$ material

### 2.1 Crystal and electrical structure

In 1954, the crystal structure of $MgB_2$ was first identified by an X-ray diffraction investigation using nickel-filtered Cu Kα radiation (Jones & Marsh, 1954). $MgB_2$ possesses the simple $AlB_2$ type structure, and its corresponding space group, crystal system, and Laue-symmetry class are P6/mmm, hexagonal, and 6/mmm, respectively. The structure consists of alternating layers of close-packed ionized $Mg^{2+}$ atoms, which are separated by honeycomb-type boron sheets. In the case of pure $MgB_2$ samples without external forcing such as hydrostatic pressure, the *a*-lattice parameter is estimated to range from ~ 3.083 to ~ 3.086 Å (Jones & Marsh, 1954; Jorgensen et al., 2001), with the variation most likely to be due to disorder in the honeycomb lattice. By contrast, the *c*-lattice parameter shows nearly the same value of ~ 3.521 Å. This may reflect the fact that in the case of close-packed hexagonal structure, the slip directions are essentially $[\bar{1}\bar{1}0]$, $[2\bar{1}0]$, and $[\bar{1}20]$ in the *ab* plane, while expansion and contraction along the *c*-axis direction hardly occurs. The fractional coordinates (*x*, *y*, *z*) for Mg and B atoms are allocated to the 1*a* site of (0, 0, 0) and the 2*d* site of (1/3, 2/3, 1/2). The site occupancies of Mg and B are observed to be ~ 0.95-1.00 and 1.00, respectively (Mori et al., 2002; Tsirelson et al., 2003; Kazakov et al., 2005). The atomic displacement parameters *U* of Mg and B atoms are also observed to be ~ 0.0049-0.0060 $Å^2$ and ~ 0.0042-0.0080 $Å^2$, respectively (Mori et al., 2002; Tsirelson et al., 2003; Kazakov et al., 2005).

Band structure calculations on $MgB_2$ (An & Pickett 2001; Kortus et al., 2001) suggest that the bands at the Fermi level ($E_F$) mainly originate from the orbitals of boron due to substantially ionized Mg, and there are four conduction bands, namely, two $\sigma$ bands delivered from the $\sigma$ bonding $2s/2p_{x,y}$ orbitals and two $\pi$ bands delivered from the $\pi$-bonding and the anti-bonding $2p_z$ orbitals. The former bands are hole types and occur in two-dimensional (2D) cylindrical forms. The latter bands are both hole type and electron type, and form three-dimensional (3D) tubular networks. The $\sigma$ states are localized and confined in the boron layers, while the $\pi$ states are delocalized in all directions. The $\sigma$ bands within boron sheets are strongly covalent, whereas the $\pi$ bands over the whole crystal show metallic behaviour, reflecting the lack of covalent bonding (Mazin & Antropov, 2003). The 2D strongly covalent states and the 3D metallic-type states mainly contribute to the total density of states (DOS) at the Fermi energy ($E_F$).

Calculations of both the band structure and the lattice dynamics for $MgB_2$ indicate that there are four distinct phonon modes at the Brillouin zone center (Γ), namely the $A_{2u}$, $B_{1g}$, $E_{1u}$, and $E_{2g}$ modes (Bohnen et al., 2001; Yildirim et al., 2001). The $A_{2u}$ singly degenerate mode involves the vibration of Mg and B layers in opposite directions along the *c* axis. The $B_{1g}$ singly degenerate mode is responsible for the vibrations of B atoms in opposite directions along the *c* axis, with the Mg atoms stationary. On the other hand, the others are doubly degenerate modes and involve only in-plane motions along the *x* or *y* axis. For the $E_{1u}$ mode, the Mg and B layers move in opposite directions. The $E_{2g}$ mode involves the vibration of the B ions in opposite directions, with the Mg ions stationary. The $E_{2g}$ in-plane boron phonons show giant anharmonicity, are strongly coupled to the $\sigma$ bands, and thus change the $2s/2px,y$ orbital overlap. The strong coupling between the holes of the $\sigma$ bands and the $E_{2g}$ mode is responsible for the high $T_c$ in $MgB_2$. The $\pi$ band charge carriers also become superconducting and

contribute to unusual superconducting behaviour in $MgB_2$ which is not observed in conventional superconductors. Since the two properties of the $\sigma$ bands are very similar and those of the $\pi$ bands are very similar, even through one $\pi$ band is hole type and the other is electron type, the electronic structure is usually simplified to one $\sigma$ band and one $\pi$ band. Therefore, $MgB_2$ is known and described as a two-band superconductor (Liu et al., 2001).

### 2.2 Unique characteristic caused by two-band and two-gap structure

$MgB_2$ is known to be theoretically and experimentally identified as the first superconductor where two superconducting gaps clearly exist (Xi, 2008; Tajima, 2005). The unique two-band and two-gap structure has an influence on the resistivity behaviour in the normal state. In the year of discovery, it became well known that the residual resistivity ratio (RRR) was independent of $T_c$ in polycrystalline $MgB_2$ samples. Specifically, many $MgB_2$ samples showed widely different RRR values despite having similar $T_c$ values around ~ 39 K (Buzea & Yamashita, 2001). In the case of the high $T_c$, the disorder effects on it (Eisterer, 2007) due to poor crystallinity and lattice strain can be negligible, and thus, the RRR value calculated from the residual resistivity was thought to depend on impurity contamination in a sample. This indicates that lower RRR is caused by a larger amount of impurity phase, even though it should be noted that the residual resistivity is partially attributable to extrinsic effects such as lack of connectivity associated with cracks, voids, and low mass density (Rowell, J. M. 2003). In the case of the two-gap superconductivity model (Golubov & Mazin, 1997), non-magnetic impurities may contribute to pair breaking, which is similar to the effects of magnetic impurities in a conventional *s*-wave superconductor. Thus, it was difficult to theoretically understand the observed unclear correlation between the RRR and the $T_c$. Regarding this issue, Mazin et al. clearly explained the mechanism by pointing out the very weak impurity scattering between the $\sigma$ and the $\pi$ bands compared with the intraband impurity scattering between the $\sigma\sigma$ and $\pi\pi$ sub-bands, due to the particular electronic structure in $MgB_2$ (Mazin et al., 2002). It was also found that the $\pi\pi$ scattering rate is larger than the $\sigma\sigma$ scattering rate. In addition, they indicated that the $T_c$ is given by the maximum eigenvalue of the superconducting coupling constant $\lambda$ for the $\sigma\pi$ and the $\pi\sigma$ interband coupling, and the $\sigma\sigma$ and $\pi\pi$ intraband coupling, while the conductivity is the sum of all the conducting channels responsible for the interband and intraband couplings. The estimated $\lambda$ for the $\sigma\sigma$ intraband coupling showed the highest value, suggesting that the $T_c$ is affected by the $\sigma$ band. These results provide the conclusion that because impurities have a stronger effect on the scattering rate of the $\pi$ band in preference to the $\sigma$ band, and thus the residual resistivity, they may not contribute to the interband scattering and $T_c$.

The upper critical field behaviour of $MgB_2$ was also found to be very different from that of a conventional phonon-mediated Bardeen, Cooper, and Schrieffer (BCS) superconductor with a single-band structure. A unique upward curvature of $B_{c2}$(T) parallel to the *ab* plane near $T_c$ was observed in single crystal $MgB_2$ samples (Zehetmayer et al., 2002; Lyard et al., 2002). This upward curvature can be well explained by using the Ginzburg-Landau theory, suggesting that the $B_{c2}$ is determined by the Ginzburg-Landau parameter and the condensation energy (Eisterer, 2007). In the case of $MgB_2$, which has the two-band structure, the total condensation energy depends on the sum of all the energies arising from the $\sigma$ band, the $\pi$ band, and the interaction between the two bands (Eisterer et al., 2005). These condensation energies in the temperature range from absolute zero to $T_c$ show different

behaviour from each other. In particular, the contribution of the $\pi$ band to the total condensation energy at 0 T in temperatures above 30 K rapidly increases, while that below 30 K is negligible. This is the reason why the $B_{c2}$(T) of $MgB_2$ shows a positive curvature near $T_c$. The unique slope can make the zero-temperature $B_{c2}(0)$ significantly higher than that estimated from a single-gap dirty superconductor model (Gurevich, 2003). In addition, an interesting scenario relating to $B_{c2}$(T) for dirty two-gap superconductors was pointed out by Gurevich (Gurevich, 2007). It is assumed that $MgB_2$ can be identified as a simple bilayer sample where two thin films corresponding to the $\sigma$ and $\pi$ bands are separated by a Josephson contact, which reflects the weak interband coupling in $MgB_2$. From the two-gap dirty-limit theory for the BCS matrix constants (Golubov et al., 2002), the temperature dependence of $B_{c2}$ is mostly determined by whether the $\sigma$ film or the $\pi$ film is dirtier. Provided that the $\pi$ film is much dirtier than the $\sigma$ film, the global $B_{c2}$(T) of the bilayer at higher temperature is mainly controlled by the $\sigma$ film with the higher $B_{c2}$, while the $\pi$ film takes over at lower temperatures. This leads to a considerable upturn in the global $B_{c2}$ curve at low temperatures, which can not be estimated from a single-gap dirty-limit superconductor. This interesting scenario for $B_{c2}$ at low temperatures delivered from the simple bilayer model is indirectly demonstrated by experimentally observed $B_{c2}$ curves for alloyed $MgB_2$ thin films (Braccini et al., 2005). Specifically, an anomalous upward curvature of $B_{c2}$(T) at low temperatures observed in a carbon-alloyed thin film provides a record high value of $B_{c2}$(4.2K) = 51 T parallel to the *ab* plane. The extrapolation of the $B_{c2}$(T) curve to $T$ = 0 K may reach over ~ 60 T, approaching the paramagnetic limit of 65 T which is calculated from the conventional BCS theory (Sarma, 1963). This value is significantly higher than those for NbTi and $Nb_3Sn$ superconductors, which are widely used in superconducting applications now. Moreover, Gurevich pointed out that given the case of electron-phonon coupling, the paramagnetic limit of $MgB_2$ is estimated to be ~ 130 T (Gurevich, 2007). This means that there is still large room for a further increase in $B_{c2}$ from optimum dirty conditions of the intraband and the interband behaviour. Therefore, we can extract a conclusion that the two-gap superconductor $MgB_2$ is suitable for superconducting applications in higher operating temperatures and fields, which can not be reached via the use of Nb-based superconducting materials.

### 2.3 Current status in development for superconducting application

Two major critical issues facing $MgB_2$ polycrystalline materials such as wires and bulks for the next generation of superconducting applications are weak grain connectivity and lack of pinning centers (Rowell, J. M. 2003; Eisterer, 2007). In order to improve rapid $J_c$ degradation caused by its weak pinning behaviour in pure $MgB_2$ wires and bulks, so far, many doping materials have been tested since the discovery of its superconductivity. The first successful dopant for this was silicon carbide (SiC) and its additive improved the irreversibility field ($B_{irr}$) and $J_c$ (Dou et al., 2002). Numerous researchers focused on the impressive results and then started to do many studies related to carbon (C) containing dopants for real superconducting applications. Even now, SiC is still known to be one of the most effective dopants for $MgB_2$ materials. Specifically, $B_{c2}$ values near 0 K for the SiC-doped $MgB_2$ wires fabricated by the *in situ* method (Sumption et al., 2005) and coated-conductors on SiC fibers prepared from hybrid physical-chemical vapor deposition (HPCVD) (Ferrando et al., 2005) were 33 T and 55 T, respectively. These values are much higher than those of NbTi and $Nb_3Sn$. Similar doping materials, nano-carbon (Soltanian et al., 2003), carbon nanotubes

(Yeoh et al., 2004), and boron carbide (Yamamoto et al., 2005a) were also found to effectively improve the in-field $J_c$ in $MgB_2$ materials. Thus, it has been found that the carbon (C) element is indispensable for superconducting applications of $MgB_2$.

From structural analysis of C-doped $MgB_2$ single crystals (Kazakov et al., 2005), the *a*-lattice parameter was observed to decrease drastically due to the C doping effect. The lattice shrinkage is most likely due to C substitution at B sites and to the difference in atomic radius between these two atoms, which may yield substitutional defects in the crystal lattice. This is because the C replacement effect accumulates in the B layer, and dislocations and its associated stacking faults may form when the accumulated strain exceeds the critical value. The existence of lattice defects in C-doped $MgB_2$ samples has been proven by experimental results (Kazakov et al., 2005; Avdeev et al., 2003; Zhu et al., 2007; Kim et al., 2012). Specifically, the considerable increase in the atomic displacement parameter at the Mg and B sites in C-doped single crystals reflects the enhancement of lattice disorder (Kazakov et al., 2005). The reason why reliability factors for Rietveld refinement in C-doped samples show high values compared with those for pure samples may be explained by the presence of local disorder in the lattice, which can not be described using conventional refined parameters (Kazakov et al., 2005; Avdeev et al., 2003). The C-doped thin films deposited by HPCVD, which shows a high $B_{c2}$ at 0 K value of 70 T, are found to have intensive structural disorder caused by dislocations (Zhu et al., 2007a). In the case of SiC-doped tapes showing relatively low mass density compared with $MgB_2$ thin films, the $MgB_2$ grains are also found to show a large amount of interior contrast generated by intragrain defects that are likely due to lattice disorder (Zhu et al., 2007b). In addition, the relationship between lattice change and not only substitutional, but also interstitial defects in C-doped $MgB_2$ materials can be theoretically explained by Vienna *ab* initio calculations (Bengtson et al., 2010). Recently, boron vacancies were clearly observed in C-doped $MgB_2$ wires and it has been found that those vacancies generate intrinsic stacking faults within the $MgB_2$ grains, together with associated lattice distortion (Kim et al., 2012). Thus, in C-doped $MgB_2$ materials, the reduced unit cell volume caused by the lattice shrinkage leads to introduction of lattice disorder effects, which result in increasing scattering of charge carriers, reducing the mean free path, and thereby enhancing $B_{c2}$ and $J_c$ (Kazakov et al., 2005; Eisterer, 2007).

However, in the case of inorganic carbon compounds as C doping materials, due to its high melting points or its high decomposition temperature, high-temperature reaction is usually required to effectively cause the lattice shrinkage of the *a*-lattice parameter. These sintering conditions generally offer the disadvantage of grain growth associated with weak grain boundary pinning, because this pinning mechanism is also known to be effective in $MgB_2$ materials (Larbalestier et al., 2001; Eisterer, 2007). To address the problem, organic compounds as C doping materials with relatively low decomposition temperatures have been intensively studied from around 2006 (Kim et al., 2006; Hossain et al., 2009; Kim et al., 2010; Maeda et al., 2011a). One of the best known organic dopants that has been suggested to date is malic acid ($C_4H_6O_5$) (Kim et al., 2006). The advantage is that the carbohydrate melts and decomposes at a low temperature below the temperature of $MgB_2$ formation. The decomposition produces highly reactive and fresh C on the atomic scale for C substitution on B site in the lattice. Due to these excellent characteristics, the *a*-lattice parameter decreases even under low-temperature sintering conditions, and grain growth is suppressed, resulting in considerable enhancement of $J_c$ and $B_{c2}$. Specifically, the $J_c$ value at

4.2 K and 6 T for *in situ* processed $C_4H_6O_5$-doped $MgB_2$ wires exceeds $1.0 \times 10^5$ A/cm$^2$, which is comparable to that for commercial NbTi wires (Kim et al., 2010). The application of cold high pressure densification to those $MgB_2$ wires yielded a high $J_c$ value of $4.0 \times 10^4$ A/cm$^2$ at 4.2 K and 10 T, which is the record value among conventional *in situ* powder-in-tube (PIT) processed $MgB_2$ wires (Hossain et al., 2009).

According to recent advanced microscopic analysis by using scanning transmission electron microscopy (STEM) and electron energy loss spectroscopy (EELS), un-reacted carbon agglomerates are found to be formed at grain boundaries in C-doped $MgB_2$ (Kim et al., 2012). The residual impurity arises from inhomogeneous mixing of starting materials including carbon compound as dopant and impedes supercurrent flow. In order to address the issue, recently, a carbon containing gas diffusion method by using oxygen-free pyrene ($C_{16}H_{10}$) was proposed (Maeda et al., 2011b). Pyrene is an aromatic hydrocarbon and its boiling temperature is 404 $^o$C lower than the temperature of $MgB_2$ formation. Owing to the characteristic, molecular carbon delinked from pyrene gas homogenously distributes into dense $MgB_2$ materials and it causes intensive structural disorder without any severe deterioration of grain connectivity. In addition, more recently, an alternative carbon doping method by using carbon encapsulated boron nanopowder made from a radio frequency plasma process was also proposed and the resultant C-doped $MgB_2$ wires showed high $J_c$ performance due to very thin carbon layers on boron surface for its carbon homogenous distribution (Kim et al., 2011). Thus, the weak flux pinning problem has been well addressed by these recent advanced carbon doping methods, resulting in considerable improvement of high-field $J_c$ of $MgB_2$.

On the other hand, the other major issue, the weak grain connectivity, has also known to be critical for the superconducting performance of $MgB_2$ since the discovery of its superconductivity (Rowell, J. M. 2003; Eisterer, 2007). This is more serious compared with the former major issue and it occurs in $MgB_2$ polycrystalline materials prepared from not only *in situ* reaction of Mg and B mixtures but also *ex situ* fabrication through the use of $MgB_2$ powder. The *in situ* PIT method is the most popular methods for fabricating $MgB_2$ conductors and the $J_c$ performance is currently higher than that of *ex situ* processed conductors. However, the *in situ* processed conductors show numerous voids caused by $MgB_2$ formation (Kim et al., 2007). This is because the theoretical volume of the mixture ($V_{Mg}$ + $V_{2B}$) is larger than the volume of the reacted $MgB_2$. The resultant mass density is limited to ~ 50 % of the theoretical density, and the porous structure significantly reduces the supercurrent-carrying area and the $J_c$ for $MgB_2$ materials. In order to counter the severe problem, *in situ* Mg diffusion methods have been proposed (Canfield et al., 2001; Kang et al., 2001) and it seems to be the most effective method even though there is still room for real application.

### 2.4 Mg diffusion method

Mg diffusion into a B matrix for fabricating dense $MgB_2$ materials was suggested by Canfield et al. and Kang et al. around the same time (Canfield et al., 2001; Kang et al., 2001), soon after the discovery of superconductivity in $MgB_2$. Canfield et al. successfully fabricated the first $MgB_2$ wire using the Mg diffusion method (Canfield et al., 2001). The specific technique was to expose boron filaments to Mg vapour or liquid at 950 $^o$C for 2 hours. The obtained conductor showed a very low residual resistivity of ~ 0.38 μΩcm and a high

density above 80 % of theoretical. Even now, $MgB_2$ conductors prepared by conventional *in situ* or *ex situ* PIT methods do not reach either value. On the other hand, Kang et al. first made high-quality $MgB_2$ thin films via a similar method (Kang et al., 2001). The successful technique was to deposit amorphous B thin films and sinter them in Mg vapor at 950 °C for 10-30 minutes. The self-field $J_c$ at 5 K for the obtained film showed a high value of ~ $6.0 \times 10^6$ A/cm² and a low residual resistivity of ~ 2.0 μΩcm, which was likely due to its highly dense structure. Thus, the Mg diffusion method was found to yield higher mass density of $MgB_2$ matrix in materials compared with conventional *in situ* PIT method, and it has been modified by many researchers for further enhancement of $J_c$ and real applications of various materials such as wires and bulks since it was first discovered (Giunchi, 2003; Ueda et al., 2005; Togano et al., 2009).

For the synthesis of dense $MgB_2$ bulks, the reactive liquid Mg infiltration (RLI) technique was proposed by Giunchi (Giunchi, 2003). The method has the advantage that desired forms can be fabricated on a large scale and in an inexpensive way without hot pressing methods. The following is a brief procedure of the fabrication method. First, compacted B powders in contact with an appropriate amount of Mg bulk pieces are inserted into steel containers with desirable shapes. The containers are arc-welded in Ar atmosphere using a high-temperature resistant technique and then sintered at 750-950 °C. After sintering, the $MgB_2$ bulks are obtained by removal of the containers. The mass density of the obtained samples is ~ 2.40 g/cm³, and the transport $J_c$ values at 4.2 K and 10 T reach $3.0 \times 10^3$ A/cm². Moreover, the RLI technique in combination with *in situ* PIT methods can be applied to the fabrication of monofilament and multifilament $MgB_2$ hollow wires (Giunchi et al., 2003). It is found that hollow cores are formed in the sintered wire due to Mg diffusion into the B matrix. The formed $MgB_2$ core was observed to have highly dense structure from SEM observation.

In order to address the problem of the low $J_c$ at self field in $MgB_2$ bulks, the powder-in-closed-tube (PICT)-diffusion method was suggested by Ueda et al. (Ueda et al., 2005). The bulks were prepared by the following procedure. The starting Mg and B powders in appropriate amounts were separately packed into a stainless steel tube. The tube was deformed into a tape-shaped sample and both ends were sealed by bending and pressing. The samples were vacuum-sealed in a silicon dioxide ($SiO_2$) tube and then sintered at 800-900 °C. The obtained sample sintered at 800 °C for 60 hours exhibits well-connected small grains with sizes of 30-100 nm. The mass density is above 95 % of the theoretical density, and the self-field $J_c$ value at 20 K reaches ~ $8.6 \times 10^5$ A/cm² due to its good connectivity.

To achieve much less MgO secondary phase, as well as highly dense structure in $MgB_2$ conductors, an interface diffusion process was proposed by Togano et al. (Togano et al., 2006). The conductors were fabricated from an interface diffusive reaction between an Fe-Mg alloy substrate and B at 950 °C for 12 hours. The formed $MgB_2$ layer was observed to be composed of densely packed equi-axial grains of submicron size and without oxygen contamination. This group also suggested an internal Mg diffusion (IMD) process for further enhancement of $J_c$ in $MgB_2$ wires (Hur et al., 2008). Specifically, 19-filament dense $MgB_2$ wires are fabricated by the internal Mg diffusion (IMD) process and the transport $J_c$ values at 4.2 K and 10 T reach ~ $1.0 \times 10^5$ A/cm² (Togano et al., 2009). This performance is the best $J_c$ reported so far in $MgB_2$ wires. However, despite these attractive performances of Mg diffusion processed materials, very little work has been done on the effects of sintering temperature on the phase composition, lattice parameters, mass density, grain size, $T_c$, $B_{c2}$,

and $J_c$ in $MgB_2$ prepared from Mg diffusion process. In this study, therefore, we have systematically evaluated structural and superconducting properties in Mg diffusion processed $MgB_2$ bulks sintered under various heat-treated conditions.

## 3. Experimental

### 3.1 Sample preparation via Mg diffusion and evaporation processes

All samples were fabricated via Mg diffusion and evaporation processes, as shown in Fig, 1.

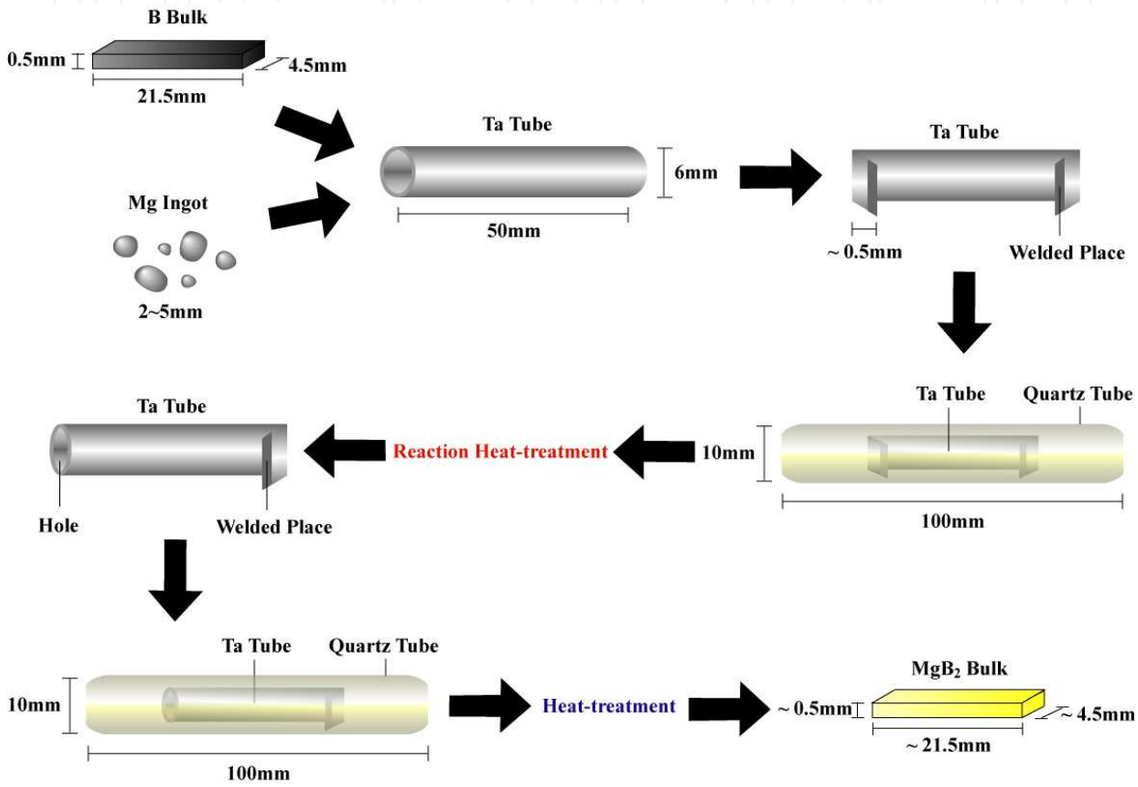


Fig. 1. Schematic diagram showing a fabrication method of $MgB_2$ via Mg diffusion and evaporation processes.

Mg ingots (purity 99.99 %, size 2-5 mm) and amorphous B powder (purity 99.995 %, size 0.25 μm) were used as starting materials and the molar ratio was chosen to be 1 : 1. The reason for using the large amount of Mg ingots is to eliminate Mg loss caused by MgO formation and to more homogeneously diffuse Mg into B matrix in comparison with what occurs in a Mg diffusion process with the stoichiometric molar ratio. Amorphous B powder was pressed into slabs with dimensions of 4.5 x 21.5 x 0.5 mm under a pressure of 100 MPa. The compacted B powder and Mg ingots were placed in a Ta tube. Both ends of the Ta tube were sealed by a metal inert gas (MIG) welding method in a glove box filled with high purity Ar gas. During the MIG welding process, the Ta tube was heat-sunk with ice-cooled copper block to avoid heating the slab and Mg ingots. The sealed Ta tube was vacuum-sealed in a quartz tube and then heat-treated under four major types of sintering conditions that are (1) an one-step sintering process at 1100 $^{o}$C which is higher than the boiling point of

Mg, (2) an one-step sintering process at 660 °C which is higher than the melting point of Mg, (3) a two-step process sintered at 1100 °C for a short period of 6 minutes followed by second sintering at 660 °C, and (4) a two-step process sintered at 660 °C for 12 hours followed by second sintering at 1100 °C. After each sintering process for $MgB_2$ formation, a large amount of unreacted Mg remains in the sealed Ta tubes. In order to remove the residual Mg from $MgB_2$ sample, the Ta tube was pierced through and again vacuum-sealed in a quartz tube to undergo an Mg evaporation process at 680 °C for 0.5 hour.

### 3.2 Sample characterization

The phase composition was investigated from X-ray powder diffraction (XRD) patterns which were collected with a Rigaku RINT 2000 diffractmeter using CuKα radiation. Rietveld refinement of the crystal structure was carried out with the RIETAN-2000 program (Izumi & Ikeda, 2000) and the structural parameters were refined by fitting the observed XRD patterns. The morphology and grain size were examined using a HITACHI S–4500 Scanning Electron Microscopy (SEM). The real and the imaginary component curves of ac susceptibility and the dc magnetization loops were evaluated by using a SQUID magnetometer (MPMS-5T, Quantum Design). The $T_c$ and $B_{c2}$ were determined by ac susceptibility measurements at $f$ = 76.97 Hz with $\mu_0 H_{ac}$ = 10 μT and $\mu_0 H_{dc}$ = 0, 0.2, 0.5, 1, 2, 3, 4, and 5 T. The $J_c$ values were derived from the magnetization hysteresis loops using the Bean critical state model (Chen & Goldfarb, 1989).

## 4. Results and discussion

### 4.1 Morphology and density

Figure 2 shows the SEM images of the surface of Mg diffusion processed samples via various sintering conditions. For reference, compacted amorphous B powder was also observed, as can be seen in Fig. 2(j). It was found that the one-step sintering process at 1100 °C yields well-developed crystalline grains, as shown in Fig. 2(a), (b), and (c). The crystal grains were also found to grow rapidly with an increase in sintering time. Specifically, the average grain sizes of samples sintered at 1100 °C for 0.5, 1, and 3 hours were observed to be approximately 0.8, 1.5, and 3.0 μm, respectively. The mass densities of the corresponding samples are 2.2, 2.4, and 1.9 g/cm$^3$, respectively, and close to the theoretical density of $MgB_2$. However, the drastic decrease in mass density from 2.4 g/cm$^3$ to 1.9 g/cm$^3$ is most likely due to the observed rapid growth caused by the increase in sintering time. It is well known that grain boundaries can act as pinning sites in $MgB_2$ materials (Larbalestier et al., 2001; Eisterer, 2007). The considerably large grains offer the disadvantage of lowering in-field $J_c$, even though high mass density is easily achieved by the one-step process at 1100 °C for the short sintering time. Contrary to the grain growth, the one-step sintering process at 660 °C for long sintering time ranging from 24 hours to 96 hours was found to leave grain size more or less the same, as can be seen in Fig. 2(d), (e), and (f). It is important to note that the average grain size is much smaller than that of Mg diffusion processed samples at 1100 °C and the grain shape shows poorly crystallized form. It is also well known that crystallinity associated with structural disorder in the lattice as well as grain boundaries can enhance the flux pinning effect (Yamamoto et al., 2005b; Eisterer, 2007). The low-temperature sintering process is advantageous in terms of both poor crystallinity and small grains.

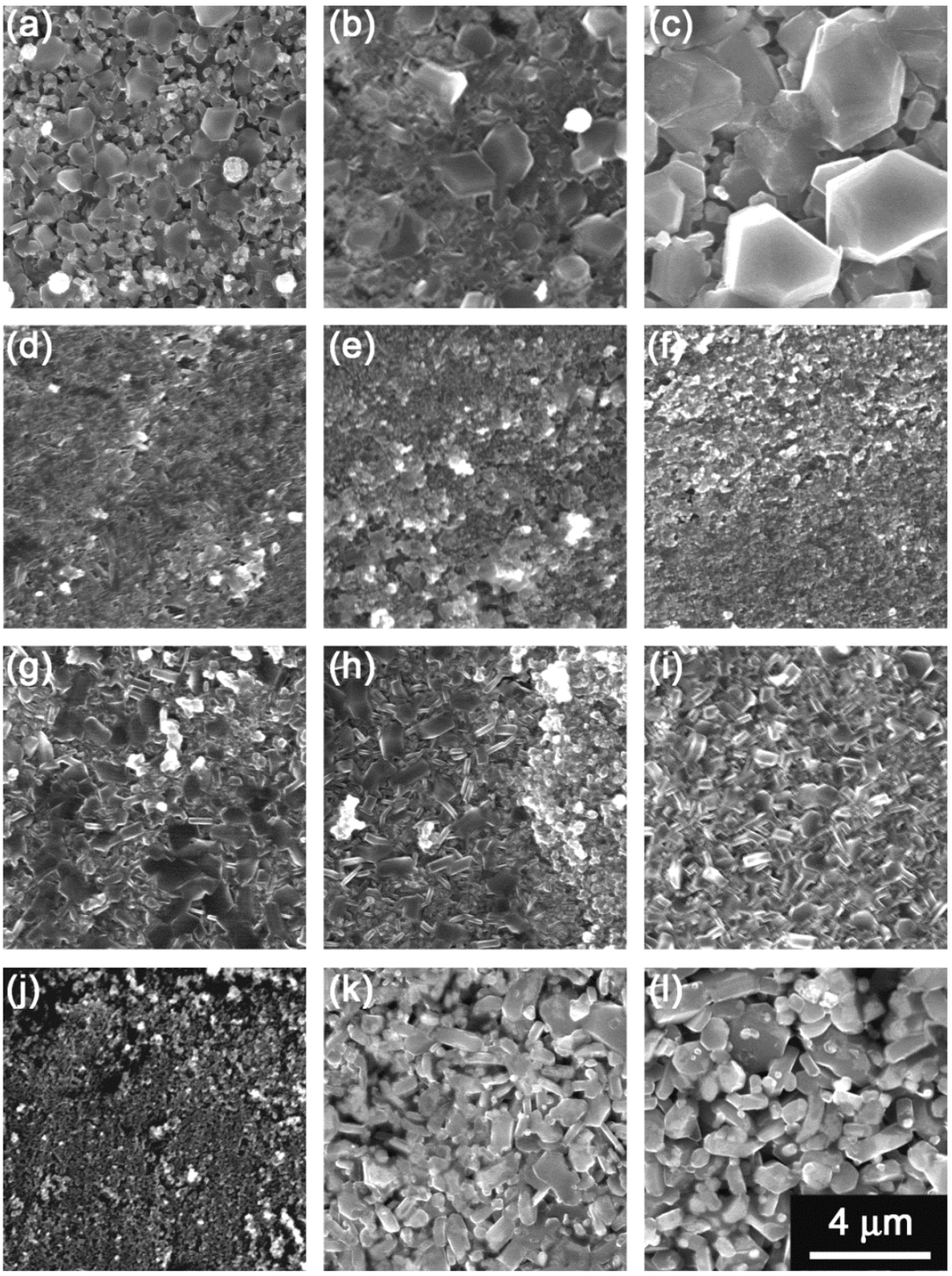


Fig. 2. Microstructure of Mg diffusion processed samples via various sintering conditions including (a) 1100 °C 0.5 h, (b) 1100 °C 1 h, (c) 1100 °C 3 h, (d) 660 °C 24 h, (e) 660 °C 48 h, (f) 660 °C 96 h, (g) 1100 °C 0.1h - 660 °C 3 h, (h) 1100 °C 0.1 h - 660 °C 6 h, (i) 1100 °C 0.1h - 660 °C 12 h, (k) 660 °C 12 h - 1100 °C 0.25 h, and (l) 660 °C 12 h - 1100 °C 0.5 h. (j) Microstructure of compacted B powder before sintering.

However, the Mg diffusion processed samples at 660 °C were brittle and the mass densities are ~ 1.5 g/cm$^3$. The value is almost half of the theoretical density, even though the SEM images of the corresponding samples seem to be dense. The porous structure caused by the low density may intensively limit grain connectivity and hence supercurrent flow. On the other hand, the two-step process first sintered at 1100 °C for 0.1 hour followed by second sintering at 660 °C for 3 -12 hours was found to form well-developed crystalline grains, as can be seen in Fig. 2(g), (h), and (i). The average grain size is below 1 μm and smaller than that of Mg diffusion processed samples via the one-step sintering at 1100 °C. However, unlike Mg diffusion processed samples via the one-step sintering at 660 °C which have small grains, the mass densities are ~ 2.4 -2.5 g/cm$^3$ and those are above 90 % of the theoretical density. The two-step sintering process achieves both high density and small grains, which arise from the natures of high-temperature sintering and low-temperature sintering, respectively. In contrast to the highly dense structure related to the well-connected small grains, the two-step process first sintered at 660 °C for 12 hours followed by second sintering at 1100 °C for 0.25 - 0.5 hour was found to result in loosely connected grains, as can be seen in Fig. 2(k) and (l). The mass densities are ~ 1.7 g/cm$^3$ and this result also confirm its porous structure. The corresponding samples were observed to have well-developed crystalline and relatively large grains. The two-step sintering process yields low-density structure and large crystal grains due to low-temperature sintering and high-temperature sintering, respectively.

### 4.2 Phase composition and lattice structure

All Mg diffusion processed samples were observed to have the same phase composition, which consists of $MgB_2$ with a trace amount of MgO from XRD $\theta$-$2\theta$ scans. Hereafter the samples will be referred as $MgB_2$ samples. In order to examine deeper insight of microstructure, structural parameters of four $MgB_2$ samples sintered via four major conditions were refined and its result is listed in Table 1. It was found that the $a$-lattice parameter is slightly changed owing to various sintering effects, while leaving the $c$-lattice parameter the same. The $a$-lattice parameter of the $MgB_2$ sample sintered at 660 °C for 48 hours shows 3. 0850 Å, and it is the lowest value of the four samples. The decrease in the $a$-lattice parameter reduces the unit cell volume of $MgB_2$. The reduction may introduce structural disorder in the lattice and decrease the DOS at the $E_F$ responsible for a considerable change in $T_c$ and thus $B_{c2}$. The XRD full width at half maximum (FWHM) is well known to be closely related to crystallite size and structural disorder and it is also listed in Table 1. The one-step sintering process at 1100 °C and the two-step process first sintered at 660 °C followed by second sintering at 1100 °C were found to obtain relatively narrow FWHM reflecting well-crystallized and large grain. This is consistent with the SEM result, as can be seen in Fig. 2. On the other hand, the FWHM values of the rest of $MgB_2$ samples were observed to be much broader than those of the other $MgB_2$ samples. The broad FWHM of the $MgB_2$ sample sintered at the one-step process at 660 °C is caused by poorly crystallized and small grains, as also indicated by the SEM observation. However, it should be noted that the FWHM of the $MgB_2$ sample first sintered at 1100 °C followed by second sintering at 660 °C is comparable to that of the sample sintered at 660 °C for 48 hours, although the corresponding sample seems to have well crystallized grains which are distinctly lager than that of $MgB_2$ samples sintered at the one-step process at 660 °C. This indicates that thanks to the second sintering at the low temperature, the two-step process could achieve both a high

level of disorder and small grains in the high-density $MgB_2$ samples, which are essential for enhancing the flux pinning effect. The MgO nanoparticles are also well known to act as pinning sites in $MgB_2$ thin films (Eom et al., 2001; Singh et al., 2008), whereas it is difficult to control the size in polycrystalline $MgB_2$ samples and large MgO grains could impede supercurrent flow (Maeda et al., 2011a). In this respect, it is necessary to eliminate the MgO impurity from polycrystalline $MgB_2$ materials. However, the MgO secondary phase of the four $MgB_2$ samples is not sensitive to sintering conditions. This indicates that even Mg diffusion process could not avoid MgO formation.

| Sintering condition | 1100°C1h | 660°C48h | 1100°C0.1h - 660°C6h | 660°C12h - 1100°C0.5h |
|---|---|---|---|---|
| X-ray powder diffraction data | | | | |
| Radiation source | CuKα | | | |
| λ (Å) | 1.54060 (CuKα$_1$), 1.54443 (CuKα$_2$) | | | |
| $\Delta 2\theta$ (°) | 0.01 | | | |
| Temperature (K) | 298 | | | |
| Goodness of fit | | | | |
| *s* | 1.32 | 1.27 | 1.23 | 1.23 |
| Lattice parameters | | | | |
| *a* (Å) | 3.0864 (2) | 3.0850 (2) | 3.0859 (2) | 3.0868 (2) |
| *c* (Å) | 3.5210 (1) | 3.5210 (1) | 3.5210 (1) | 3.5211 (2) |
| Unit cell volume | | | | |
| *V* (Å$^3$) | 29.047 (2) | 29.020 (3) | 29.038 (3) | 29.054 (3) |
| Reflection of $MgB_2$ (101) | | | | |
| FWHM(°) | 0.15 | 0.31 | 0.29 | 0.10 |
| Weight fraction | | | | |
| $MgB_2$ (wt%) | 95.9 | 95.8 | 96.3 | 96.1 |
| MgO (wt%) | 4.1 | 4.2 | 3.7 | 3.9 |

Table 1. Results of Rietveld refinement on XRD data for Mg diffusion processed samples via four major sintering conditions that are 1100 °C for 1 hour, 660 °C for 48 hours, 1100 °C for 0.1 hour followed by second sintering at 660 °C for 6 hours, and 660 °C for 12 hours followed by second sintering at 1100 °C for 0.5 hour. The fitting quality between the observed pattern and the calculated one was evaluated by goodness of fit *s*.

### 4.3 Influence on $T_c$

Figure 3 shows the real and imaginary components of the ac susceptibility for four $MgB_2$ samples sintered via four major conditions. It was found that the onset of diamagnetism at the dc field of 0 T for the $MgB_2$ sample sintered at 660 °C for 48 hours is ~ 38 K and 1 K lower than those for the other samples. The decrease in $T_c$ is most likely due to lattice disorder caused by the reduction of unit cell volume, as indicated by the refinement result listed in Table 1. It is noteworthy that although the other three samples show ~ 39 K of the onset diamagnetism at the dc field of 0 T, the superconducting transition curves are different. Specifically, the transition width of the $MgB_2$ sample first sintered at 1100 °C followed by second sintering at 660 °C is ~ 1.5 K and approximately two times broader than that of the $MgB_2$ sample sintered by the one-step process at either 1100 °C or 660 °C. It was

reported that the broad transition width arises from the nature of two kinds of superconducting $MgB_2$ phases, which are good ordering phase and a relatively lower level of ordering phase owing to the two-step sintering process (Maeda et al., 2008). The lower level of ordering phase could be a cause for the broad FWHM responsible for structural disorder, as observed in the XRD pattern (Table 1). Contrary to this, the transition width of the $MgB_2$ sample first sintered at 660 °C followed by second sintering at 1100 °C is ~ 0.3 K, suggesting that the sample consists of nearly perfect crystallite $MgB_2$ grains without any lattice disorder.

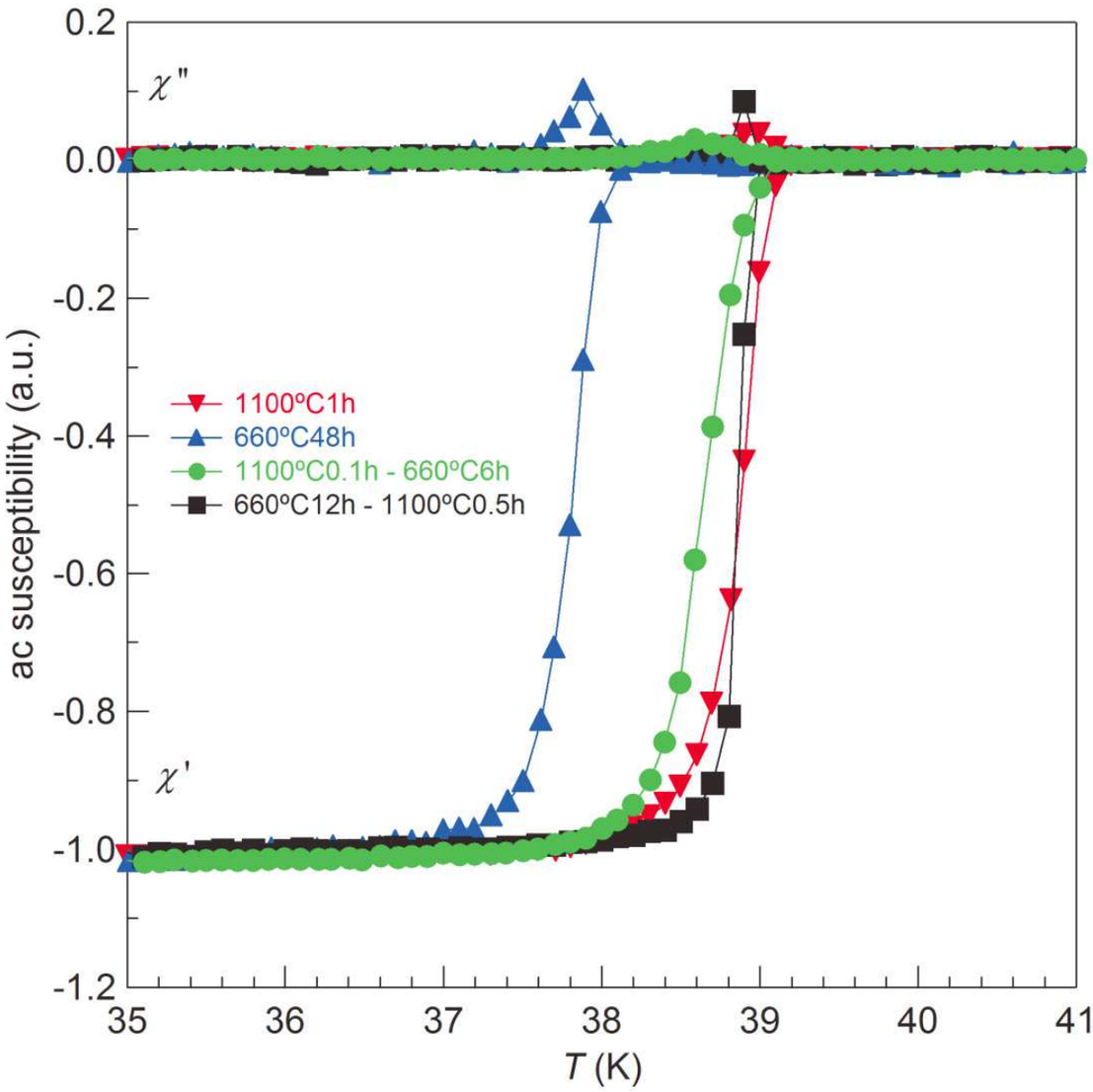


Fig. 3. The real and imaginary components of ac susceptibility with $f$ = 76.97 Hz, $\mu_0 H_{ac}$ = 10 μT, and $\mu_0 H_{dc}$ = 0 T for Mg diffusion processed samples via four major sintering conditions that are 1100 °C for 1 hour, 660 °C for 48 hours, 1100 °C for 0.1 hour followed by second sintering at 660 °C for 6 hours, and 660 °C for 12 hours followed by second sintering at 1100 °C for 0.5 hour.

### 4.4 Influence on $B_{c2}$

Figure 4 shows the temperature dependence of $B_{c2}$ for $MgB_2$ samples sintered via various conditions.

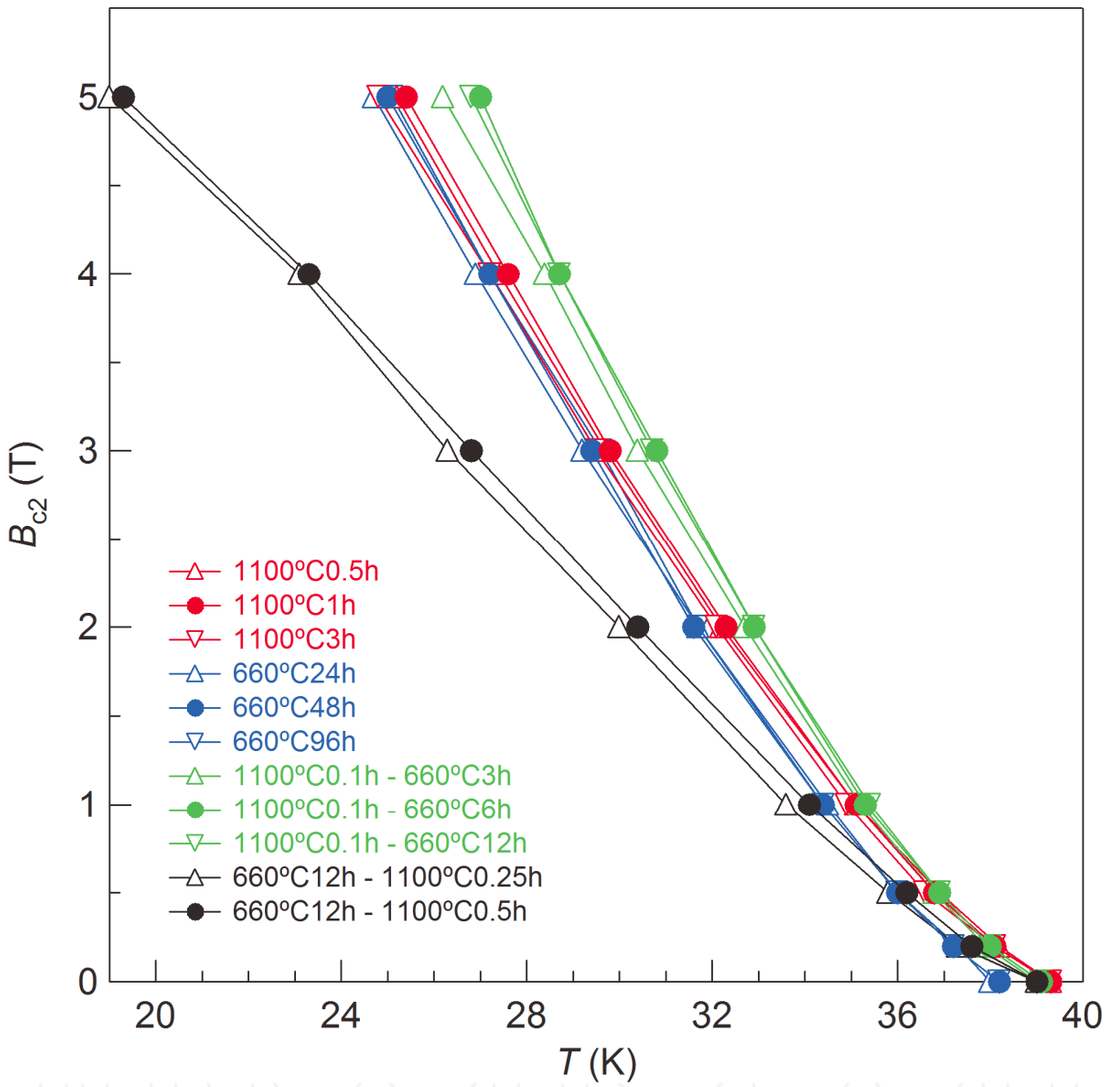


Fig. 4. The temperature dependence of $B_{c2}$ derived from ac susceptibility with $f$ = 76.97 Hz, $\mu_0 H_{ac}$ = 10 μT, and $\mu_0 H_{dc}$ = 0, 0.2, 0.5, 1, 2, 3, 4, and 5 T for $MgB_2$ samples sintered via various conditions.

It was found that although all $MgB_2$ samples has positive curvatures of $B_{c2}$ at $T \sim T_c$ reflecting suppression of the diffusivity in the $\sigma$ bands compared to that in the $\pi$ bands (Gurevich, 2003), the behaviours of curves at lower temperature are considerably different. The $B_{c2}$ slopes of the $MgB_2$ samples first sintered at 1100 ºC followed by second sintering at 660 ºC or sintered only at 660 ºC are steeper in comparison with those of the $MgB_2$ samples sintered at 1100 ºC. The structural disorder of both samples may be responsible for this. By contrast, the $B_{c2}$ slopes of the $MgB_2$ samples sintered at 660 ºC followed by second sintering

at 1100 °C are intensively shelving compared to those of the other $MgB_2$ samples. This indicates that the $MgB_2$ samples do not have any lattice defects, as suggested by the result of the narrow superconducting transition (Figure 3).

### 4.5 Influence on $J_c$

Figure 5 shows the magnetic field dependence of $J_c$ at 20 K for $MgB_2$ samples sintered via various conditions. It was found that the $J_c$ curves are highly sensitive to sintering conditions which lead to considerably differences in $MgB_2$ structure, as shown in the results of SEM observation, XRD analysis, and ac susceptibility. The most noticeable feature shown in this figure is that the in-field $J_c$ of the $MgB_2$ samples sintered at 1100 °C followed by

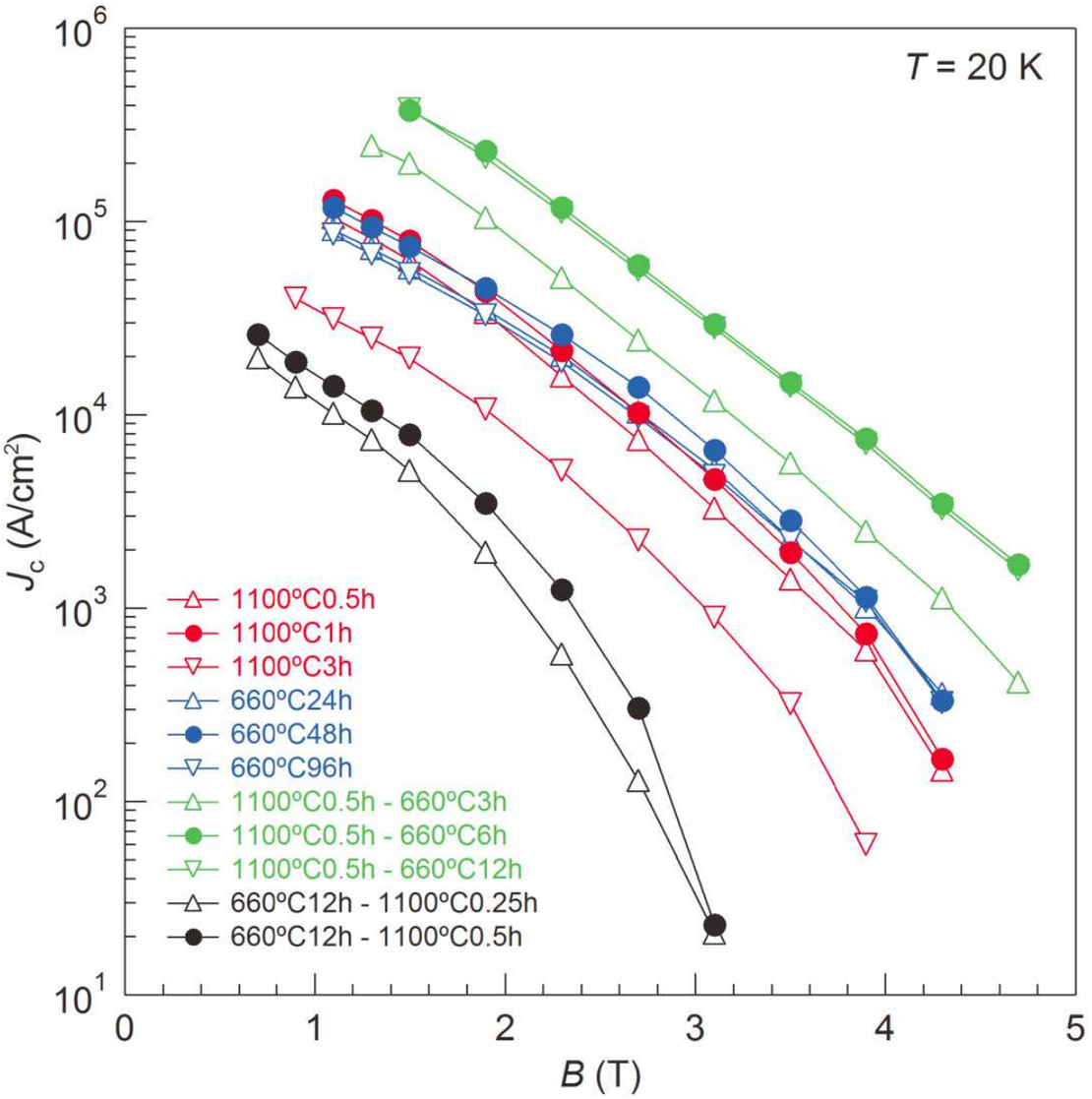


Fig. 5. Magnetic field dependence of $J_c$ at 20 K for $MgB_2$ samples sintered via various conditions.

second sintering at 660 °C is significantly higher than those of the other $MgB_2$ samples. The enhancement of $J_c$ at not only low field but also high field is clearly due to the two-step sintering process which yields well-connected small grains with a high level of disorder in highly dense $MgB_2$ samples. It is also interesting to note that even though the $J_c$ of the $MgB_2$ sample sintered at 1100 °C for 1 hour is nearly the same as that of the $MgB_2$ sample sintered at 660 °C for 48 hours, the behaviours of the curves are somewhat different. Specifically, the low-field $J_c$ of the $MgB_2$ sample sintered at 1100 °C for 1 hour is slightly higher than that of the $MgB_2$ sample sintered at 660 °C for 48 hours, whereas the corresponding behaviours of high-field $J_c$ are distinctly opposite. This results from high density and lack of pinning sites caused by good crystallinity, which are responsible for the increase in self-field $J_c$ and the decrease in high-field $J_c$, respectively. Owing to the low density and nearly perfect crystallization, the $MgB_2$ samples sintered at 660 °C followed by second sintering at 1100 °C show the lowest values of in-field $J_c$ in all $MgB_2$ samples.

## 5. Conclusion

In summary, this chapter has introduced structural characteristic and superconducting performance of pure $MgB_2$ polycrystalline samples fabricated by Mg diffusion processes. The Mg diffusion processes easily yield $MgB_2$ phase and a trace amount of MgO phase in polycrystalline samples. The microstructure and mass density of the $MgB_2$ samples can be controlled by Mg diffusion processes via various sintering conditions. The two-step sintering process, namely, the sintering for a short period of 0.1 hour at 1100 °C first, followed by the second sintering at 660 °C, produces highly dense $MgB_2$ samples characterized by well-connected small grains with a high level of disorder. The unique feature results in considerable improvement of $B_{c2}$ and in-field $J_c$. Therefore, Mg diffusion process is critical for controlling the structure of $MgB_2$ polycrystalline samples, and there is great potential for further enhancement of $J_c$ by careful optimisation of sintering conditions.

## 6. References

An, J. M. & Pickett, W. E. (2001). Superconductivity of MgB2: Covalent bonds driven metallic. *Physical Review Letters*, 86(19): 4366-4369, ISSN 0031-9007.

Avdeev, M.; Jorgensen, J. D.; Ribeiro, R. A.; Bud'ko, S. L. & Canfield, P. C. (2003). Crystal chemistry of carbon-substituted MgB2. *Physica C - Superconductivity and Its Applications*, 387(3-4): 301-306, ISSN 0921-4534.

Bengtson, A. K.; Bark, C. W.; Giencke, J.; Dai, W. Q.; Xi, X. X.; Eom, C. B. & Morgan, D. (2010). Impact of substitutional and interstitial carbon defects on lattice parameters in MgB2. *Journal of Applied Physics*, 107(2): 023902, ISSN 0021-8979.

Braccini, V.; Gurevich, A.; Giencke, J. E.; Jewell, M. C.; Eom, C. B.; Larbalestier, D. C.; Pogrebnyakov, A.; Cui, Y.; Liu, B. T.; Hu, Y. F.; Redwing, J. M.; Li, Q.; Xi, X. X.; Singh, R. K.; Gandikota, R.; Kim, J.; Wilkens, B.; Newman, N.; Rowell, J.; Moeckly, B.; Ferrando, V.; Tarantini, C.; Marre, D.; Putti, M.; Ferdeghini, C.; Vaglio, R. & Haanappel, E. (2005). High-field superconductivity in alloyed MgB2 thin films. *Physical Review B*, 71(1): 012504, ISSN 1098-0121.

Canfield, P. C.; Finnemore, D. K.; Bud'ko, S. L.; Ostenson, J. E.; Lapertot, G.; Cunningham, C. E. & Petrovic, C. (2001). Superconductivity in dense MgB2 wires. *Physical Review Letters*, 86(11): 2423-2426, ISSN 0031-9007.

Chen, D. X. & Goldfarb, R. B. (1989). Kim Model for Magnetization of Type-II Superconductors. *Journal of Applied Physics*, 66(6): 2489-2500, ISSN 0021-8979.

Dou, S. X.; Soltanian, S.; Horvat, J.; Wang, X. L.; Zhou, S. H.; Ionescu, M.; Liu, H. K.; Munroe, P. & Tomsic, M. (2002). Enhancement of the critical current density and flux pinning of MgB2 superconductor by nanoparticle SiC doping. *Applied Physics Letters*, 81(18): 3419-3421, ISSN 0003-6951.

Eisterer, M. (2007). Magnetic properties and critical currents of MgB2. *Superconductor Science & Technology*, 20(12): R47-R73, ISSN 0953-2048.

Eisterer, M.; Zehetmayer, M.; Weber, H. W. & Karpinski, J. (2005). Reversible magnetization of the two-band MgB2 superconductor: A phenomenological approach. *Physical Review B*, 72(13): 134525, ISSN 1098-0121.

Eom, C. B.; Lee, M. K.; Choi, J. H.; Belenky, L. J.; Song, X.; Cooley, L. D.; Naus, M. T.; Patnaik, S.; Jiang, J.; Rikel, M.; Polyanskii, A.; Gurevich, A.; Cai, X. Y.; Bu, S. D.; Babcock, S. E.; Hellstrom, E. E.; Larbalestier, D. C.; Rogado, N.; Regan, K. A.; Hayward, M. A.; He, T.; Slusky, J. S.; Inumaru, K.; Haas, M. K. & Cava, R. J. (2001). High critical current density and enhanced irreversibility field in superconducting MgB2 thin films. *Nature*, 411(6837): 558-560, ISSN 0028-0836.

Ferrando, V.; Orgiani, P.; Pogrebnyakov, A. V.; Chen, J.; Li, Q.; Redwing, J. M.; Xi, X. X.; Giencke, J. E.; Eom, C. B.; Feng, Q. R.; Betts, J. B. & Mielke, C. H. (2005). High upper critical field and irreversibility field in MgB2 coated-conductor fibers. *Applied Physics Letters*, 87(25): 252509, ISSN 0003-6951.

Giunchi, G. (2003). High density MgB2 obtained by reactive liquid Mg infiltration. *International Journal of Modern Physics B*, 17(4-6): 453-460, ISSN 0217-9792.

Giunchi, G.; Ceresara, S.; Ripamonti, G.; Di Zenobio, A.; Rossi, S.; Chiarelli, S.; Spadoni, M.; Wesche, R. & Bruzzone, P. L. (2003). High performance new MgB2 superconducting hollow wires. *Superconductor Science & Technology*, 16(2): 285-291, ISSN 0953-2048.

Golubov, A. A. & Mazin, I. I. (1997). Effect of magnetic and nonmagnetic impurities on highly anisotropic superconductivity. *Physical Review B*, 55(22): 15146-15152, ISSN 1098-0121.

Golubov, A. A.; Kortus, J.; Dolgov, O. V.; Jepsen, O.; Kong, Y.; Andersen, O. K.; Gibson, B. J.; Ahn, K. & Kremer, R. K. (2002). Specific heat of MgB2 in a one- and a two-band model from first-principles calculations. *Journal of Physics-Condensed Matter*, 14(6): 1353-1360, ISSN 0953-8984.

Gurevich A. (2003). Enhancement of the upper critical field by nonmagnetic impurities in dirty two-gap superconductors. *Physical Review B*, 67(18): 184515, ISSN 1098-0121.

Gurevich A. (2007). Limits of the upper critical field in dirty two-gap superconductors. *Physica C - Superconductivity and Its Applications*, 456(1-2): 160-169, ISSN 0921-4534.

Hossain, M. S. A.; Senatore, C.; Fluekiger, R.; Rindfleisch, M. A.; Tomsic, M. J.; Kim, J. H. & Dou, S. X. (2009). The enhanced Jc and Birr of in situ MgB2 wires and tapes alloyed with C4H6O5 (malic acid) after cold high pressure densification. *Superconductor Science & Technology*, 22(9): 095004, ISSN 0953-2048.

Hur, J. M.; Togano, K.; Matsumoto, A.; Kumakura, H.; Wada, H. & Kimura, K. (2008). Fabrication of high-performance MgB2 wires by an internal Mg diffusion process. *Superconductor Science & Technology*, 21(3): 032001, ISSN 0953-2048.

Izumi, F. & Ikeda, T. (2000). A Rietveld-analysis program RIETAN-98 and its applications to zeolites. *Materials Science Forum*, 321-324: 198-205, ISSN 0255-5476.

Jones, M. E. & Marsh, R. E. (1954). The Preparation and Structure of Magnesium Boride, MgB2. *Journal of the American Chemical Society*, 76(5): 1434-1436.

Jorgensen, J. D.; Hinks, D. G. & Short, S. (2001). Lattice properties of MgB2 versus temperature and pressure. *Physical Review B*, 63(22): 224522, ISSN 0163-1829.

Kang, W. N.; Kim, H. J.; Choi, E. M.; Jung, C. U. & Lee, S. L. (2001). MgB2 superconducting thin films with a transition temperature of 39 Kelvin. *Science*, 292(5521): 1521-1523, ISSN 0036-8075.

Kazakov, S. M.; Puzniak, R.; Rogacki, K.; Mironov, A. V.; Zhigadlo, N. D.; Jun, J.; Soltmann, C.; Batlogg, B. & Karpinski, J. (2005). Carbon substitution in MgB2 single crystals: Structural and superconducting properties. *Physical Review B*, 71(2): 024533, ISSN 1098-0121.

Kim, J. H.; Dou, S. X.; Shi, D. Q.; Rindfleisch, M. & Tomsic, M. (2007). Study of MgO formation and structural defects in in situ processed MgB2/Fe wires. *Superconductor Science & Technology*, 20(10): 1026-1031, ISSN 0953-2048.

Kim, J. H.; Heo, Y. U.; Matsumoto, A.; Kumakura, H.; Rindfleisch, M.; Tomsic, M. & Dou, S. X. (2010). Comparative study of mono- and multi-filament MgB2 wires with different boron powders and malic acid addition. *Superconductor Science & Technology*, 23(7): 075014, ISSN 0953-2048.

Kim, J. H.; Oh, S.; Heo, Y. U.; Hata, S.; Kumakura, H.; Matsumoto, A.; Mitsuhara, M.; Choi, S.; Shimada, Y.; Maeda, M.; MacManus-Driscoll, J. L. & Dou, S. X. (2012). Microscopic role of carbon on MgB2 wire for critical current density comparable to NbTi. *NPG Asia Materials*, 4: ISSN(online) 1884-4057.

Kim, J. H.; Oh, S.; Kumakura, H.; Matsumoto, A.; Heo, Y. U.; Song, K. S.; Kang, Y. M.; Maeda, M.; Rindfleisch, M.; Tomsic, M.; Choi, S & Dou, S. X. (2011) Tailored materials for high performance MgB2 wire. *Advanced Materials*, 23(42): 4942-4946, ISSN 0935-9648.

Kim, J. H.; Zhou, S.; Hossain, M. S. A.; Pan, A. V. & Dou, S. X. (2006). Carbohydrate doping to enhance electromagnetic properties of MgB2 superconductors. *Applied Physics Letters*, 89(14): 142505, ISSN 0003-6951.

Kortus, J.; Mazin, I. I.; Belashchenko, K. D.; Antropov, V. P. & Boyer, L. L. (2001). Superconductivity of metallic boron in MgB2. *Physical Review Letters*, 86(20): 4656-4659, ISSN 0031-9007.

Larbalestier, D.; Gurevich, A.; Feldmann, D. M. & Polyanskii, A. (2001). High-Tc superconducting materials for electric power applications. *Nature*, 414(6861): 368-377, ISSN 0028-0836.

Liu, A. Y.; Mazin, I. I. & Kortus, J. (2001). Beyond Eliashberg superconductivity in MgB2: Anharmonicity, two-phonon scattering, and multiple gaps. *Physical Review Letters*, 87(8): 087005, ISSN 0031-9007.

Lyard, L.; Samuely, P.; Szabo, P.; Klein, T.; Marcenat, C.; Paulius, L.; Kim, K. H. P.; Jung, C. U.; Lee, H. S.; Kang, B.; Choi, S.; Lee, S. I.; Marcus, J.; Blanchard, S.; Jansen, A. G. M.; Welp, U.; Karapetrov, G. & Kwok, W. K. (2002). Anisotropy of the upper critical field and critical current in single crystal MgB2. *Physical Review B*, 66(18): 180502, ISSN 1098-0121.

Maeda, M.; Kim, J. H.; Kumakura, H.; Heo, Y. -U.; Zhao, Y.; Nakayama, Y.; Rindfleisch, M. & Dou, S. X. (2011a). Influence of hydrogen-containing argon gas on the structural parameters and superconducting properties of malic acid-doped MgB2 wires. *Scripta Materialia*, 64(11): 1059-1062, ISSN 1359-6462.

Maeda, M.; Kim, J. H.; Zhao, Y.; Heo, Y. U.; Takase, K.; Kubota, Y.; Moriyoshi, C.; Yoshida, F.; Kuroiwa, Y. & Dou, S. X. (2011b). In-field Jc improvement by oxygen-free pyrene gas diffusion into highly dense MgB2 superconductor. *Journal of Applied Physics*, 109(2): 023904, ISSN 0021-8979.

Maeda, M.; Zhao, Y.; Dou, S. X.; Nakayama, Y.; Kawakami, T.; Kobayashi, H. & Kubota, Y. (2008). Fabrication of highly dense MgB2 bulk at ambient pressure. *Superconductor Science & Technology*. 21(3): 032004, ISSN 0953-2048.

Mazin, I. I. & Antropov, V. P. (2003). Electronic structure, electron-phonon coupling, and multiband effects in MgB2. *Physica C - Superconductivity and Its Applications*, 385(1-2): 49-65, ISSN 0921-4534.

Mazin, I. I.; Andersen, O. K.; Jepsen, O.; Dolgov, O. V.; Kortus, J.; Golubov, A. A.; Kuz'menko, A. B. & van der Marel, D. (2002). Superconductivity in MgB2: Clean or dirty?. *Physical Review Letters*, 89(10): 107002, ISSN 0031-9007.

Mori, H.; Lee, S.; Yamamoto, A.; Tajima, S. & Sato, S. (2002). Electron density distribution in a single crystal of Mg1-xB2 [x=0.045(5)]. *Physical Review B*, 65(9): 092507, ISSN 1098-0121.

Nagamatsu, J.; Nakagawa, N.; Muranaka, T.; Zenitani, Y. & Akimitsu, J. (2001). Superconductivity at 39 K in magnesium diboride. *Nature*, 410(6824): 63-64, ISSN 0028-0836.

Rowell, J. M. (2003). The widely variable resistivity of MgB2 samples. *Superconductor Science & Technology*, 16(6): R17-R27, ISSN 0953-2048.

Sarma, G. (1963). On the influence of a uniform exchange field acting on the spins of the conduction electrons in a superconductor. *Journal of Physics and Chemistry of Solids*, 24(8): 1029-1032.

Singh, R. K.; Shen, Y.; Gandikota, R.; Carvalho, C.; Rowell, J. M. & Newman, N. (2008). Effect of oxygen incorporation on normal and superconducting properties of MgB2 films. *Applied Physics Letters*, 93(24): 242504, ISSN 0003-6951.

Soltanian, S.; Horvat, J.; Wang, X. L.; Munroe, P. & Dou, S. X. (2003). Effect of nano-carbon particle doping on the flux pinning properties of MgB2 superconductor. *Physica C - Superconductivity and Its Applications*, 390(3): 185-190, ISSN 0921-4534.

Sumption, M. D.; Bhatia, M.; Rindfleisch, M.; Tomsic, M.; Soltanian, S.; Dou, S. X. & Collings, E. W. (2005). Large upper critical field and irreversibility field in

MgB2 wires with SiC additions. *Applied Physics Letters*, 86(9): 092507, ISSN 0003-6951.

Tajima, S. (2005). Two-gap superconductivity in MgB2. *Agne Gijutsu Center Solid State Physics*, 40(1): 1-12, ISSN 0454-4544.

Togano, K.; Hur, J. M.; Matsumoto, A. & Kumakura, H. (2009). Fabrication of seven-core multi-filamentary MgB2 wires with high critical current density by an internal Mg diffusion process. *Superconductor Science & Technology*, 22(1): 015003, ISSN 0953-2048.

Togano, K.; Nakane, T.; Fujii, H.; Takeya, H. & Kumakura, H. (2006). An interface diffusion process approach for the fabrication of MgB2 wire. *Superconductor Science & Technology*, 19(6): L17-L20, ISSN 0953-2048.

Tsirelson, V.; Stash, A.; Kohout, M.; Rosner, H.; Mori, H.; Sato, S.; Lee, S.; Yamamoto, A.; Tajima, S. & Grin, Y. (2003). Features of the electron density in magnesium diboride: reconstruction from X-ray diffraction data and comparison with TB-LMTO and FPLO calculations. *Acta Crystallographica Section B -Structural Science*, 59(5): 575-583, ISSN 0108-7681.

Ueda, S.; Shimoyama, J.; Iwayama, I.; Yamamoto, A.; Katsura, Y.; Horii, S. & Kishio, K. (2005). High critical current properties of MgB2 bulks prepared by a diffusion method. *Applied Physics Letters*, 86(22): 222502, ISSN 0003-6951

Xi, X. X. (2008). Two-band superconductor magnesium diboride. *Reports on Progress in Physics*, 71(11): 116501, ISSN 0034-4885.

Yamamoto, A.; Shimoyama, J.; Ueda, S.; Iwayama, I.; Horii, S. & Kishio, K. (2005a). Effects of B4C doping on critical current properties of MgB2 superconductor. *Superconductor Science & Technology*, 18(10): 1323-1328, ISSN 0953-2048.

Yamamoto, A; Shimoyama, J; Ueda, S; Katsura, Y; Horii, S. & Kishio, K. (2005b). Improved critical current properties observed in MgB2 bulks synthesized by low-temperature solid-state reaction. *Superconductor Science & Technology*, 18(1): 116-121, ISSN 0953-2048.

Yeoh, W. K.; Horvat, J.; Dou, S. X. & Keast, V. (2004). Strong pinning and high critical current density in carbon nanotube doped MgB2. *Superconductor Science & Technology*, vol. 17(9): S572-S577, ISSN 0953-2048.

Yildirim, T.; Gulseren, O.; Lynn, J. W.; Brown, C. M.; Udovic, T. J.; Huang, Q.; Rogado, N.; Regan, K. A.; Hayward, M. A.; Slusky, J. S.; He, T.; Haas, M. K.; Khalifah, P.; Inumaru, K. & Cava, R. J. (2001). Giant Anharmonicity and Nonlinear Electron-Phonon Coupling in MgB2: A Combined First-Principles Calculation and Neutron Scattering Study. *Physical Review Letters*, 87(3): 037001, ISSN 0031-9007.

Zehetmayer, M.; Eisterer, M.; Jun, J.; Kazakov, S. M.; Karpinski, J.; Wisniewski, A. & Weber, H. W. (2002). Mixed-state properties of superconducting MgB2 single crystals. *Physical Review B*, 66(5): 052505, ISSN 1098-0121.

Zhu, Y.; Larbalestier, D. C.; Voyles, P. M.; Pogrebnyakov, A. V.; Xi, X. X. & Redwing, J. M. (2007a). Nanoscale disorder in high critical field, carbon-doped MgB2 hybrid physical-chemical vapor deposition thin films. *Applied Physics Letters*, 91(8): 082513, ISSN 0003-6951.

Zhu, Y.; Matsumoto, A.; Senkowicz, B. J.; Kumakura, H.; Kitaguchi, H.; Jewell, M. C.; Hellstrom, E. E.; Larbalestier, D. C. & Voyles, P. M. (2007b). Microstructures of SiC nanoparticle-doped MgB2/Fe tapes. *Journal of Applied Physics*, 102(1): 013913, ISSN 0021-8979.

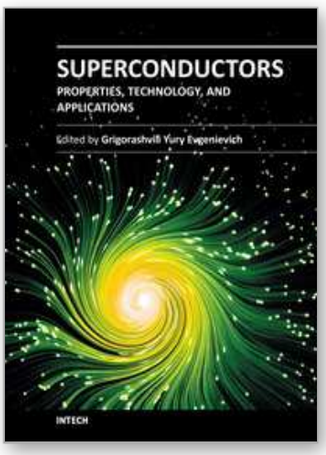


**Superconductors - Properties, Technology, and Applications**
Edited by Dr. Yury Grigorashvili

ISBN 978-953-51-0545-9
Hard cover, 436 pages
**Publisher** InTech
**Published online** 20, April, 2012
**Published in print edition** April, 2012

Book "Superconductors - Properties, Technology, and Applications" gives an overview of major problems encountered in this field of study. Most of the material presented in this book is the result of authors' own research that has been carried out over a long period of time. A number of chapters thoroughly describe the fundamental electrical and structural properties of the superconductors as well as the methods researching those properties. The sourcebook comprehensively covers the advanced techniques and concepts of superconductivity. It's intended for a wide range of readers.



**InTech Europe**
University Campus STeP Ri
Slavka Krautzeka 83/A
51000 Rijeka, Croatia
Phone: +385 (51) 770 447
Fax: +385 (51) 686 166
www.intechopen.com

**InTech China**
Unit 405, Office Block, Hotel Equatorial Shanghai
No.65, Yan An Road (West), Shanghai, 200040, China
中国上海市延安西路65号上海国际贵都大饭店办公楼405单元
Phone: +86-21-62489820
Fax: +86-21-62489821

IntechOpen